ACS OMEGA

http://pubs.acs.org/journal/acsodf

Article

Osteopontin-Targeted and PPARδ-Agonist-Loaded Nanoparticles Efficiently Reduce Atherosclerosis in Apolipoprotein E$^{-/-}$ Mice

Xu Huang, Yang Zhang, Weiwei Zhang, Cheng Qin, Yan Zhu, Yan Fang, Yabin Wang, Chengchun Tang,* and Feng Cao*

Cite This: *ACS Omega* 2022, 7, 28767−28778

Read Online

ACCESS | Metrics & More | Article Recommendations | Supporting Information

ABSTRACT: Atherosclerosis is the leading cause of vascular pathologies and acute cardiovascular events worldwide. Early theranostics of atherosclerotic plaque formation is critical for the prevention of associated cardiovascular complications. Osteopontin (OPN) expression in vascular smooth muscle cells (VSMCs) has been reported as a promising molecular target for the diagnosis and treatment of atherosclerotic plaques. The PPARδ agonist GW1516 has been shown to inhibit VSMC migration and apoptosis. However, GW1516 has low aqueous solubility and poor oral bioavailability, which are major obstacles to its broad development and application. In this study, GW1516@NP-OPN, which is anti-OPN-targeted and loaded with the PPARδ agonist GW1516, was synthesized using a nanoprecipitation method. The uptake of GW1516@NP-OPN was examined using fluorescence microscopy and flow cytometry assay in VSMC in vitro models. Using the Transwell assay and acridine orange/ethidium bromide staining methods, we observed that the inhibition of VSMCS migration and apoptosis was significantly higher in cells treated with GW1516@NP-OPN than those treated with free GW1516. The western blot assay further confirmed that GW1516@NP-OPN can increase FAK phosphorylation and TGF-βprotein expression. The effect of NPs was further tested in vivo. The atherosclerotic lesion areas were greatly decreased by GW1516@NP-OPN compared with the free drug treatment in apolipoprotein E$^{-/-}$ mice models. Consequently, our results showed that GW1516@NP-OPN stabilizes the PPARδ agonist aqueous formulation, improves its anti-plaque formation activities in vivo and in vitro, and can therefore be recommended for further development as a potential anti-atherosclerotic nanotherapy.

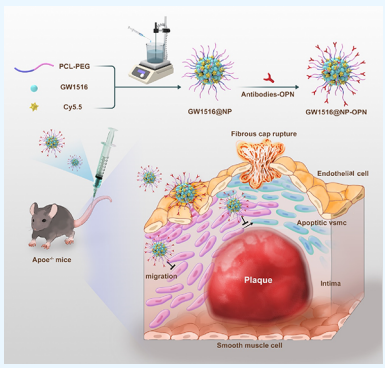

1. INTRODUCTION

Atherosclerosis, a chronic and complex cardiovascular pathology, is the leading cause of cardiovascular-related deaths worldwide.[1] Most of the early stage atherosclerotic patients can demonstrate only few clinical symptoms before the plaque becomes vulnerable and leads to sudden death.[2,3] Although the use of statin lipid-lowering therapeutic drugs was proven effective in these patients, statin therapy can also result in significant side effects including liver damage and myopathy.[4] Therefore, the question how to improve atherosclerosis-targeting therapy for early stage plaque patients and decrease potential therapy side effects remains a great challenge for healthcare systems and scientists around the world.

Higher expression levels of osteopontin (OPN) have been found in vascular smooth muscle cells (VSMCs) in atherosclerotic plaques.[5,6] Notably, VSMC migration and apoptosis are critical markers of atherosclerosis progression.[7−9] VSMC-targeting strategies represent an effective method for selective delivery of anti-atherosclerotic drugs.[10] Recent studies have shown that some small molecules can inhibit the progression of atherosclerotic plaque via correction of the abnormal VSMC behavior in plaques. For instance, the activation of the peroxisome proliferator-activated receptor δ (PPARδ) was shown to inhibit both the VSMC migration in plaques and VSMC apoptosis induced by the oxidized low-density lipoprotein (LDL). The mechanism is mediated by the transforming growth factor beta/focal adhesion kinase (TGF-β/FAK) signaling pathway.[11−13] It has been confirmed that GW1516, the most efficient agonist of PPARδ, activates strong anti-atherosclerotic effects in mice in vivo.[14] However, the efficiency of this agent is hindered by its low bioavailability and adverse side effects in other tissues such as which induced cancer in several organs in rodents, and its development in clinical research is limited.[15,16] Therefore, the development of a novel drug delivery method with lower systemic toxicity is required. Accordingly, nanomedicine was explored in this study that aims to improve the anti-atherosclerosis drug delivery system.

Received: January 28, 2022
Accepted: August 2, 2022
Published: August 15, 2022

Emerging nanotechnology employs methods that can integrate diagnostic procedures and treatment of a specific disease at the molecular level. Nanodrugs were suggested as a more advantageous tool considering their easier and more efficient absorption by target cells, lower toxicity, and improved bioavailability.[17] Recently, specific strategies were proposed on how to encapsulate the PPARγ agonist in lactic-co-glycolic acid polyethylene glycol nanoparticles.[16] In the current study, the PPARδ agonist GW1516 was encapsulated in polymeric nanoparticles (NPs) constructed of poly ε-caprolactone coupled to PEG (PCL-PEG) and coupled with the anti-OPN IgG antibody (GW1516@NP-OPN) by a coprecipitation method. Furthermore, in this study, various characteristics of nanoparticles were described including the size, surface charge, and encapsulation efficiency. GW1516 release from NPs into physiological medium, its uptake by VSMCs, and the encapsulated agent's anti-atherosclerotic behaviors were evaluated using the apolipoprotein $E^{-/-}$ ($ApoE^{-/-}$) mice model in vivo and in VSMCs in vitro.

2. METHODS

2.1. Materials and Animals. GW1516 and Cy 5.5 were purchased from Selleckchem (Boston, USA). Poly(ε-caprolactone)-poly(ethylene glycol) and maleimide-functionalized poly(ε-caprolactone)-b-poly(ethylene glycol) were purchased from Xi'an Ruixi Biological Technology Co., Ltd. (Xian, China). The mouse aortic smooth muscle (MOVAS) cells were bought from Honsun Biologicals (Shanghai, China). Dulbecco's modified Eagle's medium (DMEM) and fetal bovine serum (FBS) were procured from HyClone (Logan, UT, USA). Polyclonal rabbit anti-FAK and anti-phospho-FAKY 397 antibodies were provided by BD Transduction Laboratories (San Diego, CA, USA). Polyclonal antibodies specifically for TGF-β1, OPN, MMP-2, MMP-9, and GADH were from Biosynthesis Biotechnology Co. Ltd. (Beijing, China). Acridine orange/ethidium bromide (AO/EB), detection reagents, annexin V-FITC/PI, and western blot reagents were bought from Amersham Life Science/Beijing Solarbio Science and Technology Co. Ltd. (Beijing, China). These chemicals were of analytical grade or high-performance liquid chromatography (HPLC) grade, and, therefore, were used without further purification. Mice with $ApoE^{-/-}$ gene knockout (with the background of C57/B) were purchased from Vital River Laboratory Animal Technology Co., Ltd. (Beijing, China). The mice handling procedures were approved by the Ethics Committee of Chinese PLA General Hospital (Beijing) and were designed in agreement with the Guidance for Caring and Using Laboratory Animals Published by the US National Institutes of Health.[19]

2.2. Preparation of GW1516@NP-OPN. To prepare GW1516-PCL-PEG NPs, we used the classical coprecipitation method, which was described previously.[20] According to the protocol, 4 mg of polymer mPEG-PCL, 1 mg of polymer mal-PEG-PCL, 0.5 mg of entrapped GW1516, and 80 μg of Cy5.5 were combined in 1 mL of tetrahydrofuran and methanol (v/v, 1:1) for dissolution.[21] These materials were then mixed under ultrasonic vibration for 30 s and added dropwise to 10-fold volume of deionized water under intense agitation. After a period of overnight stirring, the NP suspension was filtered through a 220 μm microporous membrane to eliminate residual molecules. Anti-OPN antibodies were conjugated with GW1516@NP according to the methods described previously.[22] Accordingly, 2 μL of 2-mercaptoethylamine•HCl was added to 20 μL of OPN antibody, and the reaction system was catalyzed by 5 mM EDTA. Following this, the mixture had been shaken for 90 min at room temperature to generate free sulfhydryl groups in the antibody. Afterward, the solution was left to stir for 12 h at room temperature and allowed the antibody to join the GW1516@NP. Following this, high-speed centrifugation was used to remove the unattached antibody.

2.3. Characterization of GW1516@NP-OPN. Briefly, the solution was diluted with deionized water and then 10 μL of the sample was dripped on to a carbon-coated copper mesh. After water evaporation, the sample was counterstained with 5 μL of 1% phosphotungstic acid solution for 60 s and dried by a 42 °C constant temperature dryer. Finally, transmission electron microscopy (TEM) (JEM-2100) was used to measure the morphology and dimensions of GW1516@NP-OPN. A Zetasizer Nano ZS dynamic light scattering (DLS) instrument (Malvern Zetasizer 2000, Malvern, UK) was used to assess the hydrodynamic dimensions, polydispersity, and ζ potential of GW1516@NP-OPN and GW1516@NP in aqueous solutions.[23]

2.4. Measurements of the Encapsulation Efficiency, Loading Content, and Drug Release In Vitro. The actual quantity of GW1516 in NPs was tested spectrophotometrically. To measure the encapsulation percentage (EP %) and loading efficiency (LE %), a standard curve of GW1516 content in methanol was established first. Afterward, 10 mg of dried NPs was mixed with 15 mL of methanol and the mixture had been sonicated for 5 min. After filtering the solution through a filter (0.22 μm) to remove the polymer precipitates, the drug content of the filtered sample was measured using spectrophotometry. The EP % and LE % were calculated using eqs 1 and 2 below, respectively.[24]

$$\mathrm{EP} = (\text{amount of drug(mg) measured in the drug} - \text{loaded NPs/amount of drug(mg) initially used for preparing NPs}) \times 100\% \quad (1)$$

$$\mathrm{LE} = (\text{amount of drug(mg) measured in the drug} - \text{loaded NPs/amount of drug} - \text{loaded NPs (mg)}) \times 100\% \quad (2)$$

The drug release from GW1516@NP-OPN and drug-free NP (control) was measured. NPs were diluted in 9 mL of PBS (0.1% sodium dodecyl sulphate) (pH value = 7.4) and incubated in a vibrating water bath at the speed of 130 rpm at 37 °C. After incubation for 0−50 h, the samples were centrifuged at 20,000 g for 15 min and mixed with the 9 mL of PBS (0.1% SDS). Following this, the concentration of drug in the supernatant was measured by a spectrophotometer, and the cumulative amount of GW1516 release from the control or GW1516@NP-OPN was plotted as the release ratio versus time of release.

2.5. Cell Culture-Based In Vitro Experimental Procedures. *2.5.1. Cell Culture.* Primary mouse vascular aortic smooth muscle (MOVAS) cells were cultured in DMEM medium supplemented with FBS (10%) and penicillin−streptomycin (1%). The cells were cultivated in culture bottles at 37 °C in standard cell culture incubators with CO_2 (5%). The culture medium was replaced daily, and cells were subcultured at 100% confluence. The cells were treated with ox-

https://doi.org/10.1021/acsomega.2c00575
ACS Omega 2022, 7, 28767−28778

LDL at the final concentrations of 60 and 150 μg/ml. Cells between 4th and 10th passages were used in these experiments.

2.5.2. Immunofluorescence Analysis. The NP-treated cells were incubated with ox-LDL at the final concentration of 60 μg/mL for 24 h. After trypsinization and centrifugation, the cells were fixed with paraformaldehyde (4%) and washed three times with ice-cold PBS supplemented with Triton X-100 (0.2%). Following this, the cells were incubated with primary anti-OPN antibodies in PBS (with 0.1% BSA) for 1 h, washed three times in PBS, and incubated with secondary FITC-conjugated antibodies at 37 °C for 1 h. Cell nuclei were stained with DAPI. The expression of the target protein was analyzed using a confocal microscope (CLSM 510; Carl Zeiss; Germany).[23]

2.5.3. NP Cellular Uptake and Their Targeting Efficiency. MOVAS cells were cultured at an initial concentration of 10^4 cells/well in confocal dishes and incubated for 24 h with ox-LDL at the final concentration of 60 μg/ml, Following this, the medium was replaced with a medium that contained GW1516@NP or GW1516@NP-OPN. Four hours later, the medium was removed and the cells were fixed with paraformaldehyde (4%). The cell nuclei were stained with DAPI for 10 min. Following this, the cells were washed with PBS three times and tested using a two-channel confocal microscope (LSM 510; Carl Zeiss; Germany) pre-set for DAPI and Cy5.5 (466 nm excitation, 650−700 nm detection). To validate NP cellular uptake and targeting efficiency, an excitation wavelength of 650−700 nm was used to perform flow cytometry (Gallios; Beckman Coulter; CA, USA) with 10^4 MOVAS cells.[25]

2.5.4. Transwell Cell Migration and Scratch Test. The cells were cultured in six-well plates and incubated with GW1516, GW1516@NP-OPN, GW1516@NP, and drug-free NP. The final concentration of GW1516 was 100 nmol/ml in all treatments. A 100 μL cell suspension (5×10^5cells/ml in DMEM without FBS) in 1 mL medium containing 60 μg/mL ox-LDL was added to the upper chamber (pore size, 8 μm) and lower chamber of a Transwell system supplemented with DMEM containing 20% FBS. The medium and unmigrated cells in the upper chamber were discharged after 6 h. After washing the upper chamber with PBS three times, 2 mL of 4% paraformaldehyde was used to fix the cells in the lower chamber for 15 min. Crystal violet solution (0.1%) was used for staining the cells for 30 min. An OLYMPUS CX 31 microscope was used for cell counting.[26]

The wound scratch test was conducted as described previously.[27] The cells were incubated with GW1516@NP-OPN or drug-free NP for 24 h, seeded, and left to grow until cells reached 100% confluency; a scratch was done using a pipette tip. PBS was used to wash off the detached cells. Ox-LDL was used to stimulate the cells for 12 h. During the test, cells were incubated in serum-free medium. The wound at the beginning and at the end of the experiment was photographed using a light microscope. Five fields were randomly selected under the microscope for counting.

2.5.5. Apoptosis Flow Cytometry Assay. The cells were cultured in 60 mm culture dishes and treated with GW1516, GW 1516@NP-OPN, GW1516@NP, or control NP for 24 h. Following this, cells were incubated with ox-LDL (150 μg/mL) or nLDL with or without the above-mentioned NP reagents for 24 h. Apoptosis was detected using the Annexin V-FITC PI kit (Solarbio, Beijing, China) as described previously.[28]

2.5.6. Acridine Orange/Ethidium Bromide Staining. Cells were grown in 48-well plates and treated with the indicated doses of nanodrug and ox-LDL. The treated cells were washed with PB and the mixture of acridine orange/ethidium bromide as described previously (100 μg/mL of AO and EB).[29] The mixture was added gently by pipetting. Cells were assessed under the fluorescence microscope.

2.5.7. Western Blot Analysis. Western blot analysis was conducted according to the previously described protocol.[30] All proteins were extracted using radioimmunoprecipitation assay (RIPA) buffer (100 μL) and phenylmethylsulfonyl fluoride (PMSF, 1 μL). The extracted proteins were quantified using the BCA protein assay (Pierce Biotechnology; MA, USA). The samples were separated using sodium dodecyl sulphate-polyacrylamide gel electrophoresis (SDS-PAGE) and transferred to nitrocellulose membranes. The membranes were sealed with 5% (w/v) bovine serum albumin (BSA) at room temperature for 30 min.[18,31,50] The Sealed membranes were incubated with appropriate primary and secondary antibodies. The super-signal west picochemiluminescent substrate kit (Pierce Biotechnology; MA, USA) was used for blot development. ImageJ software (National Institutes of Health; USA) was used for image analysis.

2.6. Animal Experiments. *2.6.1. Atherosclerosis Mice Model In Vivo.* To test the NP ant-atherosclerotic effects in vivo, ApoE gene knockout mice were used. To develop atherosclerosis, mice were fed with high-fat (0.2% cholesterol and 21% fat) diet for 16 weeks. Control group mice were kept on normal diet (CHD). Each group consisted of five mice.[22] All animal experimental procedures were designed according the Guidance for Caring and Using of Laboratory Animals (published by the US National Institutes of Health) and approved by the Ethics Committee at the Chinese PLA General Hospital (Beijing).[32]

2.6.2. Fluorescence Imaging with GW1516@NP-OPN In Vivo. GW1516@NP-OPN was injected into mouse tail veins. The same amount of Cy 5.5 GW1516@NP was administered to the control group mice. At 675 nm excitation, the 695 nm emission from the bilateral carotid arteries was collected at 2, 6, 18, and 36 h after injection with the IVIS Lumina XR System (Caliper Life Sciences, Hopkinton, USA). The animals' carotid arteries and aorta were excised after fluorescence imaging. Following this, Living Image software (4.4) (Caliper Life Sciences, Hopkinton, USA) was used to analyze signal intensities as described previously.[33]

2.6.3. Immunohistochemistry Analysis. Isolated aortas and carotid arteries were fixed with 4% paraformaldehyde after washing with PBS. The harvested and fixed tissues were embedded in paraffin compound and then sectioned with a cryostat. The slides were then stained with hematoxylin/eosin (Sigma), Sirius red, OPN, and Masson as described previously.[34] The visualization and morphometric analysis of digitized images were conducted using ImagePro software (ImagePro Plus 7.0, Silver spring, USA).

2.7. Statistical Analysis. All data were presented as mean ± standard deviation (SD), and results were analyzed by SPSS 25 software. To compare multiple group means, we performed one-way ANOVA with a Tukey HSD test, if equal variances were assumed or Dunnett's C Post Hoc test, if equal variances were not assumed. The comparison between two groups were performed using a two-tailed unpaired Student's *t*-test, assuming a Gaussian distribution. $P < 0.05$ was considered as statistically significant.

https://doi.org/10.1021/acsomega.2c00575
ACS Omega 2022, 7, 28767−28778

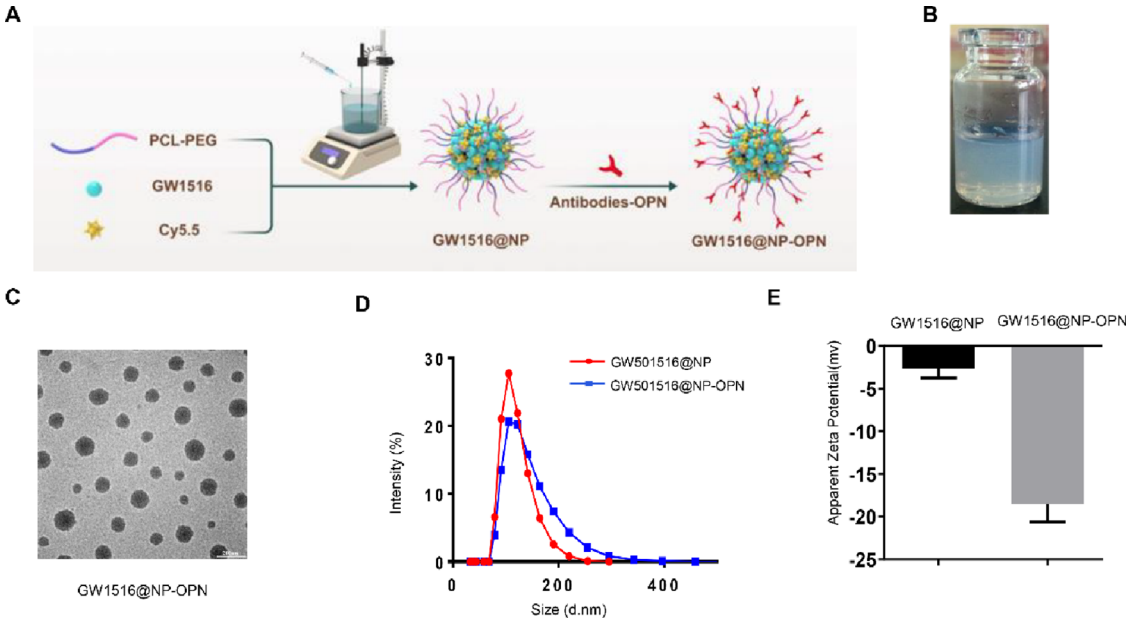

Figure 1. Characterization of nanoparticles. (A) Chemical structure of GW1516@NP-OPN. (B) Appearance of GW1516@NP-OPN suspension. (C) TEM image showing the representative photograph of GW1516@NP-OPN; bar = 100 nm. (D) Hydrodynamic diameters (E) and ζ potentials for GW1516@NP-OPN and GW1516@NP.

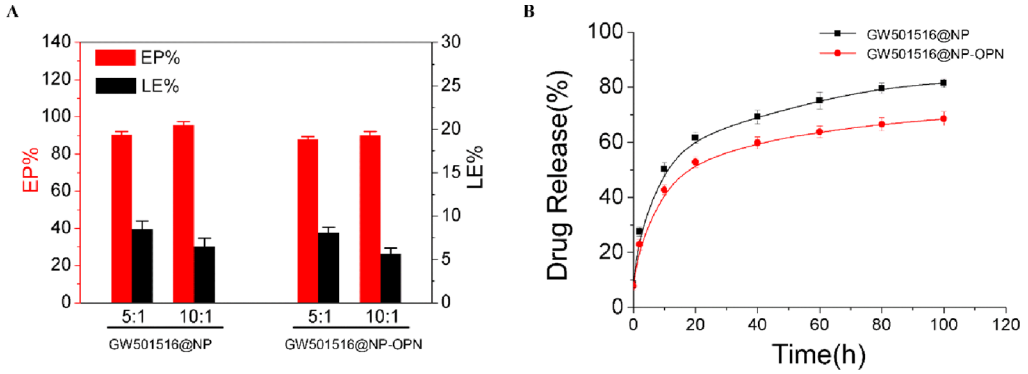

Figure 2. (A) EP % and LE % of GW1516@NP-OPN and GW1516@NP with different weight ratios of PCL-PEG to GW1516 (5:1 and 10:1). (B) In vitro release profile of GW1516 from NPs. Values are presented as mean ± SD (n = 3).

3. RESULTS

3.1. NP Characterization. The design and preparation of GW1516@NP-OPN are shown in (Figure 1A). NPs self-assembled from PCL-PEG were designated GW1516@NP; subsequently, hybrid NPs self-assembled from Cy5.5 and antibody of OPN were designated GW1516@NP-OPN. The appearance of GW1516@NP-OPN dispersed in water is shown in (Figure 1B). The optimized TEM image (Figure 1C) shows that GW1516@NP-OPN was homogeneously dispersed in aqueous solution with a well-defined spherical shape. The size ranges of the GW1516@NP-OPN shown in TEM were 80−110 nm. The DLS results indicated that the mean diameters of both the NP types were 142.5 ± 3.06 nm (GW1516@NP-OPN) and 102.0 ± 2.75 nm (GW1516@NP), respectively, with a relatively narrow size distribution indicated by PDI values of 0.25 and 0.17 (Figure 1D). Notably, we can see that the hydrodynamic diameter of the nanoparticles is significantly larger than that obtained from TEM observation. Link to antibodies of OPN appeared to contribute to the inequality in size of GW1516@NP-OPN based on the observation that targeted NPs were larger than the non-targeted NPs. According to research, another important parameter, that is, poly dispersity index (PDI), that is close to 1.0, often indicates that the nanoparticles have a very wide size distribution, which displays that the colloidal system is heterogeneous.[35] The PDIs of both GW1516@NP and GW1516@NP-OPN were less than 0.3, evidenced as colloids of monodisperse systems. The ζ potentials for GW1516@NP-OPN and GW1516@NP were −18.1 ± 0.46 mV and 0 mV, respectively (Figure 1E), suggesting that GW1516@NP-OPN had superior stability compared to non-targeted nanoparticles due to the existence of electrostatic repulsion that might prevent particle aggregation.

3.2. Encapsulation Percentage, Loading Efficiency, and Drug Release. EP % and LE % of GW1516@NP-OPN and GW1516@NP with different weight ratios of PCL-PEG to GW1516 (5:1 & 10:1) were calculated in the process of nanoprecipitation (Figure 2A). Generally, the nanoparticles show low EP % but high LE % with a decreased weight ratio (increased GW1516 concentration). Both groups of nanoparticles showed slightly higher LE % with the weight ratio of 5:1. The GW1516@NP-OPN group was shown to reach

https://doi.org/10.1021/acsomega.2c00575
ACS Omega 2022, 7, 28767−28778

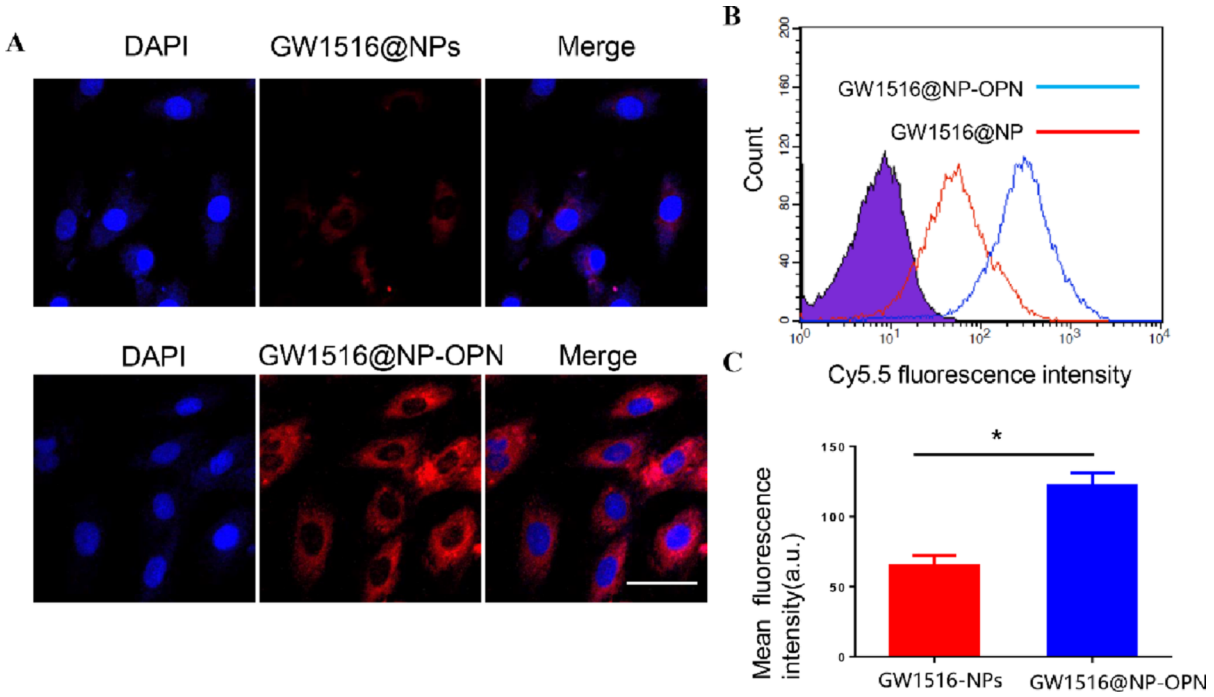

Figure 3. Intracellular uptake of GW1516@NP-OPN and non-targeted NPs by MOVAS cells in vitro. (A) To determine the uptake of the NPs, MOVAS cells were pre-treated for 24 h with ox-LDL (60 μg/mL) and then incubated with GW1516@NP-OPN or GW1516 @NP for 4 h. The DAPI channel shows blue fluorescence; middle column Cy 5.5 shows red fluorescence; merged channel shows DAPI and Cy 5.5 combined images; scale bars = 50 μm. (B) Flow cytometry analyses of MOVAS cells pre-treated for 24 h with ox-LDL (60 μg/mL) and with GW1516@NP-OPN or GW1516@NP for 4 h. (C). Mean Cy 5.5 fluorescence intensities of the NP uptake by MOVAS cells were measured using flow cytometry. The values are presented as means ± SD (n = 3); *p < 0.05.

8.06% ± 0.61 in LE %, and the GW1516@NP group was 8.5% ± 0.95 in LE %. The degree of EP % reduction in the OPN-targeted group was not found significant when the weight ratio of GW1516 to PCL-PEG changed from 10:1 to 5:1. Therefore, the ratio 5:1 was selected for NP production in further experiments.

The drug release from the nanoparticle system is a complex process, which could be attributed to drug diffusion in nano-micelle construction, which is affected by constituents and surface properties of the nano-micelles and the physicochemical properties of the drugs. According to the data shown in (Figure 2B), in vitro GW1516 release from the nanoparticles exhibits typically biphasic release patterns. GW1516 release from GW1516@NP-OPN and GW1516@NP shows an initial burst of 22.87 ± 2.00 and 27.53 ± 1.67% in the first two h, respectively. Following this, the drug release was slower reaching a plateau. The total amounts of drug released by GW1516@NP-OPN and GW1516@NP were 68.50% ± 2.53 and 81.51% ± 1.55 after 100 h, respectively. As shown in the figure, the drug release of the OPN-targeted NP group was slower than that of the non-targeted NPs. Suggestively, anti-OPN antibody conjugation may result in higher micelle density.[36]

3.3. Cellular Uptake and Targeting Efficiency of GW1561@NP-OPN. To assess the NP improved efficiency in the treatment of arteriosclerosis, the in vitro MOVAS cell model was used. NP uptake examination was conducted to evaluate intracellular levels of GW1516@NP-OPN. MOVAS cells were pre-treated for 24 h with ox-LDL (60 μg/mL) and then incubated with GW1516@NP-OPN NPs or GW1516@NP for 4 h. Cellular uptake was evaluated using a confocal laser scanning microscope (CLSM) and flow cytometry assays. Our data indicates that GW1516@NP-OPN uptake was significantly higher than that of the non-targeted NPs (Figure 3A). Accordingly, the fluorescence intensity of intracellular Cy5.5 was significantly higher for GW1516@NP-OPN compared with the non-targeted NP (Figure 3B). The mean fluorescence intensities of intracellular GW1516@NP-OPN was approximately 1.7-fold higher (p < 0.05) than those of GW1516@NP (Figure 3C).

3.4. GW1561@NP-OPN Inhibited Ox-LDL-Induced MOVAS Cell Invasion and Migration Capacity. Transwell migration chambers were used to evaluate GW1561@NP-OPN capacity to inhibit the invasion of MOVAS cells induced by ox-LDL. First, MOVAS cells were pre-treated with ox-LDL (60 μg/mL) for 24 h. Afterward, cells were treated with GW1516@NP-OPN for 24 h and left to migrate across a transwell membrane. Following this (12 h later), cells were stained using crystal violet solution for 30 min and counted using a light microscope. The migrated cells were counted in five randomly selected fields. We observed less MOVAS cells penetrating the filters after GW1516@NP-OPN treatment compared with free GW1516 and GW1516@NP (Figure 4A,B). To further assess the migration of MOVAS in vitro, a scratch assay was used. After 0 or 12 h, the cell migration images were obtained near the scratched edge. After 12 h exposure, the wound gap in the cultures exposed to GW1561@NP-OPN was significantly wider than that in the cultures treated with free GW1516 or GW1516@NP controls (Figure 4C,D).

3.5. GW1516@NP-OPN Inhibits Ox-LDL-Induced Apoptosis in MOVAS Cells. To test whether GW1516@NP-OPN can more effectively inhibit ox-LDL-induced MOVAS cell apoptosis, the cell death was examined using

https://doi.org/10.1021/acsomega.2c00575
ACS Omega 2022, 7, 28767−28778

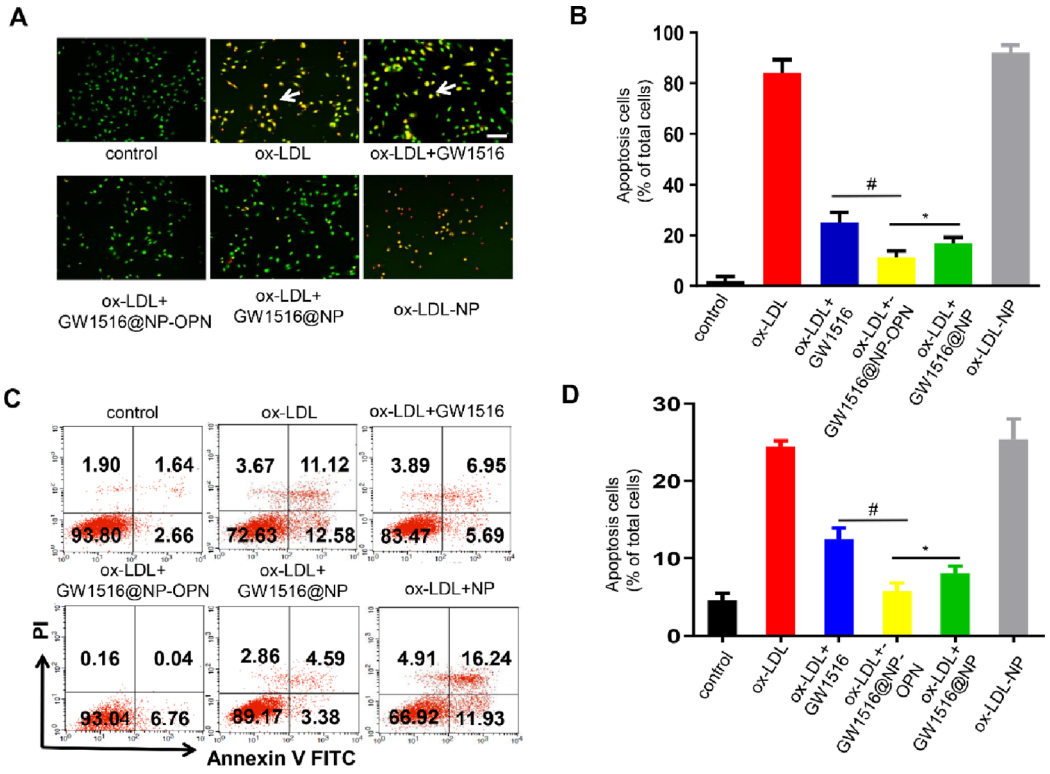

Figure 4. Transwell invasion chamber and scratch tests were used to evaluate the effect of GW1516@NP-OPN on the invasion and migration of MOVAS cells treated for 24 h with ox-LDL (60 μg/mL). (A) Transwell migration assay showing that GW1516@NP-OPN slowed down the invasion of MOVAS induced by ox-LDL compared to the effects induced by of GW1516@NP or GW1516; scale bars = 100 μm. (B) Quantification of the Transwell invasion chamber assay shown as bar graphs; #$p < 0.05$ vs the ox-LDL + GW1516 group and *$p < 0.05$ vs the ox-LDL + GW1516@NP-OPN group. (C). Scratch test data indicates that anti-OPN-GW1516@NP induces the slower migration of MOVAS cells treated with ox-LDL for 24 h compared to the effects induced by GW1516@NP or GW1516; scale bars = 100 μm. (D) Quantification of scratch test data shown as bar graphs. Data are expressed as a percentage of control. Values are expressed as means ± SD ($n = 3$). *$P < 0.05$ indicates that there is a statistically significant difference between effects produced by ox-LDL + G1516@NP and ox-LDL + GW1516@NP-OPN treatments in MOVAS cells. #$P < 0.05$ indicates that there is a statistically significant difference between effects produced by ox-LDL + GW1516 and ox-LDL + GW1516@NP treatments in MOVAS cells.

flow cytometry method dual staining assay with AO/EB staining and annexin V-FITC/PI. First, the cell apoptosis was tested using dual detection of AO/EB, in which apoptotic cells are marked by orange chromatin fragments.[37] Activation of apoptosis was detected in the control and the ox-LDL + NP-treated groups. However, the GW1516@NP-OPN treatment indicated significantly lower quantity of apoptotic cells (Figure 5A,B).

Annexin V-FITC/PI staining data show that GW1516@NP-OPN could induce lower levels of apoptosis in MOVAS cells treated with ox-LDL (150 μg/mL) for 24 h compared to the effects induced by GW1516@NP and GW1516 (Figure 5C), demonstrating the early apoptotic cells in the top right quadrant and the late apoptotic cells - in the bottom right quadrant. Ox-LDL (150 μg/mL) induced apoptosis in 24.5 ± 0.75% of the control cells. In cells treated with GW1516@NP-OPN, the apoptotic cell percentage was significantly lower (5.7% ± 1.10%) (Figure 5D).

3.6. Effect of GW1516@NP-OPN on the Expression of Proteins That Can Modulate Ox-LDL-Induced Migration and Apoptosis in MOVAS Cells. It has been demonstrated that ox-LDL can increase syntheses of MMP-2 and MMP-9 in VSMCs, cause transformation of VSMCs phenotype, and stimulate VSMCS migration.[38,39] In this study, treatment with drug alone or non-OPN-targeted NP accelerated the matrix metalloprotease MMP-2 and MMP-9 protein expressions, while GW1516@NP-OPN produced the lower degree effect (Figure 6A). Moreover, PPARδ was shown to mediate ox-LDL-induced apoptosis in VSMCs via activation of TGF-β/FAK signaling axis.[14] According to previously published data, dephosphorylation of FAK^{Y397} was associated with initiation of apoptosis.[40] Therefore, western blotting method was used to assess FAK phosphorylation levels in cells treated with ox-LDL. It is shown in (Figure 6B) that Ox-LDL can markedly suppress FAK phosphorylation. Notably, GW1516@NP-OPN reversed the negative effect of ox-LDL on FAK phosphorylation. The effect is more substantial than that of GW1516@NP or GW1516.

It has been also shown that ligand-activated PPARδ regulates ox-LDL-induced apoptosis at least in part via its influence on the dephosphorylation of FAK^{Y397} downstream of the TGF-β signaling pathway [12]. In our experiments, GW1516@NP-OPN more substantially increased TGF-β expression levels in cells treated with ox-LDL compared to GW1516@NP-OPN or GW1516 (Figure 6C).

3.7. Fluorescence Imaging of GW1516@NP-OPN Effects In Vivo and Ex Vivo. ApoE$^{-/-}$ atherosclerotic and control mice were injected intravenously with GW1516@NP-OPN or GW1561@NP, and Cy5.5 near-infrared (NIR) fluorescence (NIRF) images were obtained at different time points in vivo. The arterial fluorescence signal was significantly higher in mice injected with GW1516@NP-OPN compared

https://doi.org/10.1021/acsomega.2c00575
ACS Omega 2022, 7, 28767−28778

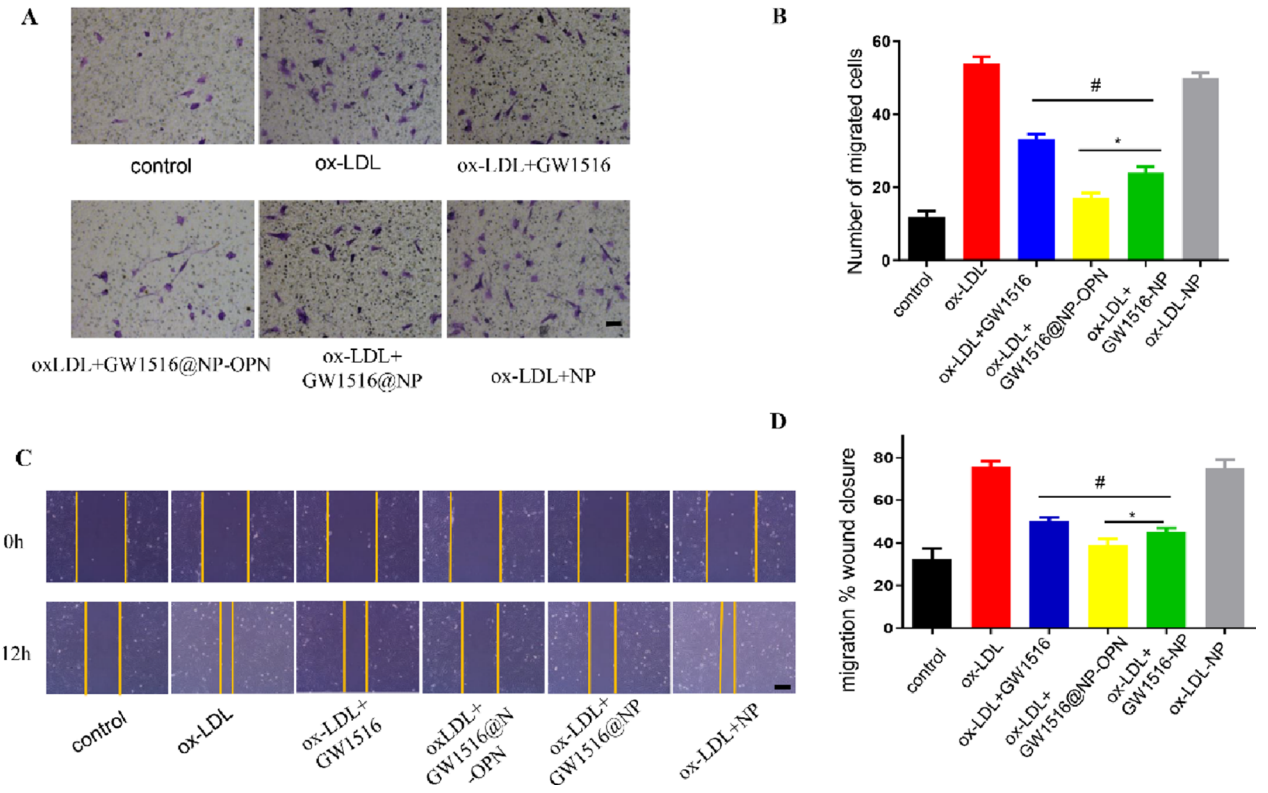

Figure 5. Effects of GW1516@NP-OPN on apoptosis was tested in ox-LDL-stimulated MOVAS cells using flow cytometry and AO/EB staining. (A) MOVAS cells were treated with PBS, ox-LDL (150 μg/ml), ox-LDL + GW1516, ox-LDL + GW1516@NP-OPN, ox-LDL + GW1516@NP, or ox-LDL + NP. Morphological apoptosis was observed using AO/EB staining (marked by yellow-orange colors); scale bars = 100 μm. (B) Bar graphs showing the quantified data for AO/EB staining. (C) Percentage of early apoptotic cells was 6.76% in the group treated with GW1516@NP-OPN. (D) Quantification of flow cytometry data shown as bar graphs. All data are presented as means ± SD of three experiments. *P < 0.05 indicates a statistically significant difference between ox-LDL + GW1516@NP and ox-LDL + GW1516@NP-OPN treatment groups. #P < 0.05 indicates a statistically significant difference between ox-LDL + GW1516@NP-OPN and ox-LDL + GW1516 treatment groups.

with GW1516@NP-injected mice (Figure 7A). Following this, Cy5.5 NIRF imaging was performed again with freshly isolated aortic tissues ex vivo. The ex vivo NIRF confirmed the data observed in vivo (Figure 7B).

3.8. Effects of GW1516@NP-OPN on the Regression of Atherosclerosis In Vivo. Effects of GW1516@NP-OPN on atherosclerosis development were analyzed in ApoE$^{-/-}$ mice fed with high fat diet for 16 w. The mice were randomly divided into five groups and treated with PBS, free GW1516, GW1516@NP, or GW1516@NP-OPN (all injections contained 3.3 mg/kg GW1516). Injections were introduced through the tail vein four times weekly for 2 weeks. Animals were sacrificed and whole aortas were excised for plaque area analysis using H&E, Sirius red, OPN, and Masson staining. H&E, Sirius red, OPN, and Masson staining of aortic sections show that the lesions were significantly smaller (decreased plaque size observed in Figure 8A, P < 0.05 GW1516@NP-OPN groups vs PBS group. The red dotted line and the blue dotted line represent the vascular intima and the fibrous cap, respectively. The plaques were located between red and blue lines.) with a smaller OPN content. Then, we examined the effect of GW1516 on the increasing of TGF-β within atherosclerotic lesions. As revealed by western blot results, GW1516@NP-OPN markedly increased the expression of TGF-β in the plaque area (P < 0.05, Figure 8C), indicating the in vivo targeted delivery of the loaded drug GW1516 to atherosclerotic lesions.

4. DISCUSSION

The formation of foam cells and the thinning of the fibrous cap of the plaque play a major role in atherosclerotic plaque rupture, which is a major cause of heart attack and stroke. The migration and apoptosis of VSMCs are the risk factors for them.[41] The ability to reduce the biological changes of VSMCs is an attractive approach to combat the initiation and progression of atherosclerotic plaque. Previous studies have shown that peroxisome proliferator-activated receptor delta (PPARδ), a ligand-activated transcription factor, was activated with synthetic agonists, which could inhibit VLDL-induced triglyceride accumulation and inflammation.[42] Similarly, Hwang JS et al. reported that PPARδ activation inhibited ox-LDL-induced apoptosis of VSMCSs.[14] However, whether PPARδ can play a beneficial role in atherosclerosis by regulating the migration and apoptosis of oxidized low-density lipoproteins is not yet fully known and the effect of treatment is also affected by pharmacokinetic profiles and drug efficiencies. Nanotechnology provides new opportunities and advanced strategies for the diagnosis and treatment of a variety of diseases including infectious diseases, malignancies, and cardiovascular pathologies.[43,44] In the previous work, due to the overexpression of OPN in activated VSMCs, compared with small molecules, the ICG/SRT@HSA-pept NMs we formulated has the functional advantage of targeting drug delivery to plaques, so the therapeutic effect is more significant.[45] In this study, we designed and constructed targeted nanoparticles combined with PPARδ receptor agonist

https://doi.org/10.1021/acsomega.2c00575
ACS Omega 2022, 7, 28767−28778

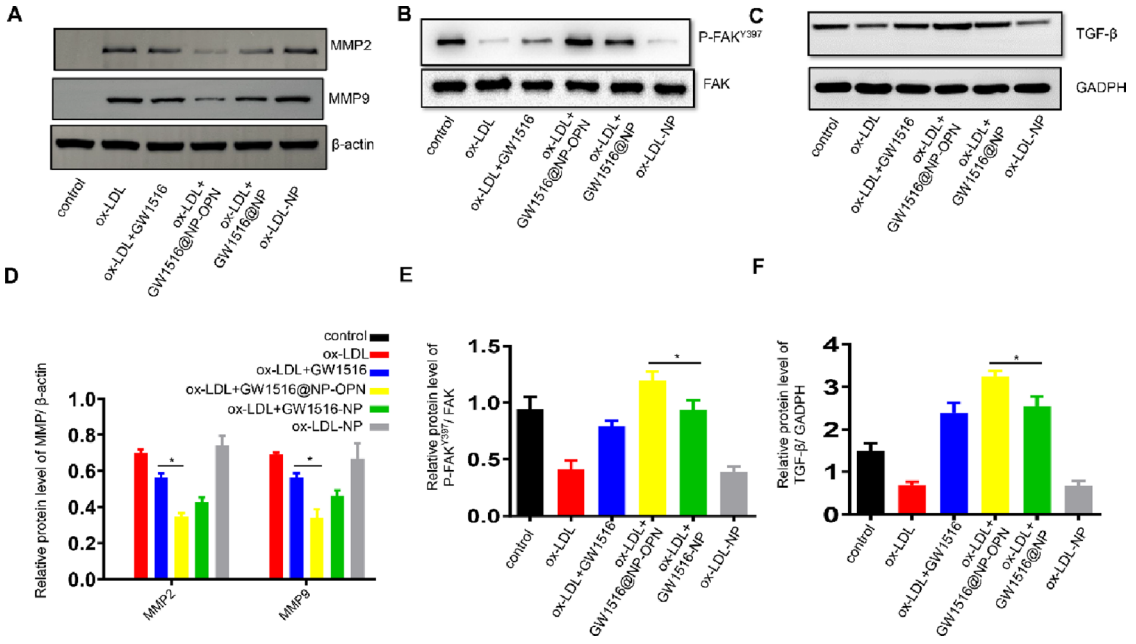

Figure 6. GW1516@NP-OPN modulates expression levels of migration and apoptosis-related proteins in MOVAS cells. MMP2/MMP9 and TGF-β/FAK expression was tested using western blotting. MOVAS cells was treated with ox-LDL (150 μg/mL for 24 h). The treated cells were incubated with PBS, GW1516, GW1516@NP-OPN, GW1516@NP, and NPs for 24 h. The expression levels of MMP-2, MMP-9 (A), TGF-β/FAK (B), and (C) were tested and visualized in total cell lysate using specific antibodies as described in the Methods section. Data are presented as mean ± SD of three experiments. *P < 0.05 indicates a statistically significant difference between ox-LDL + GW1516 and ox-LDL + GW1516@NP-OPN@NP. #P < 0.01 indicates a statistically significant difference between ox-LDL and ox-LDL + GW1516. (D–F) are the quantitative results of (A–C).

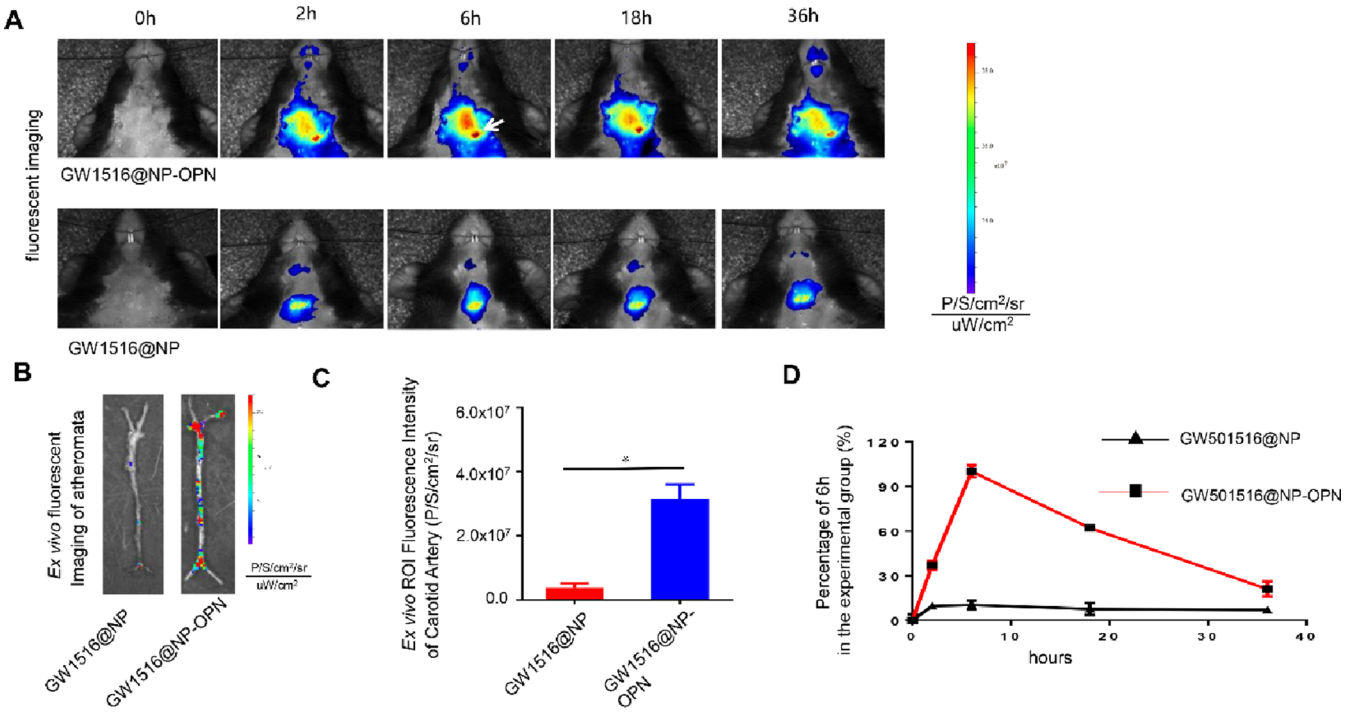

Figure 7. In vivo and ex vivo near-infrared fluorescence (NIRF) imaging of atheroma burden in ApoE$^{-/-}$ mice after the intravenous injection of GW1516@NP-OPN or GW1516@NP. (A) In vivo NIR fluorescence imaging of atheroma in ApoE$^{-/-}$ mice 0, 2, 6, 8, 18, and 36 h after intravenous injections of GW1516@NP-OPN or GW1516@NP (n = 5 per group). (B). Deposition of GW1516@NP-OPN in an artery confirmed using ex vivo NIR fluorescence imaging. (C) is the quantitative result of B. (D) is the quantitative result of A.

(GW1516@NP-OPN) that demonstrated effective inhibition of migration and apoptosis in ox-LDL-induced smooth muscle cells. Collectively, the targeting nanoparticles functioned as efficient theranostic nanomedicines for atherosclerotic plaques.

Our data supports that NPs have a high potential of achieving an improved therapeutic effect of PPARδ receptor agonist GW1516 in the treatment of atherosclerosis. The targeted NPs we designed have many advantages of specific

https://doi.org/10.1021/acsomega.2c00575
ACS Omega 2022, 7, 28767–28778

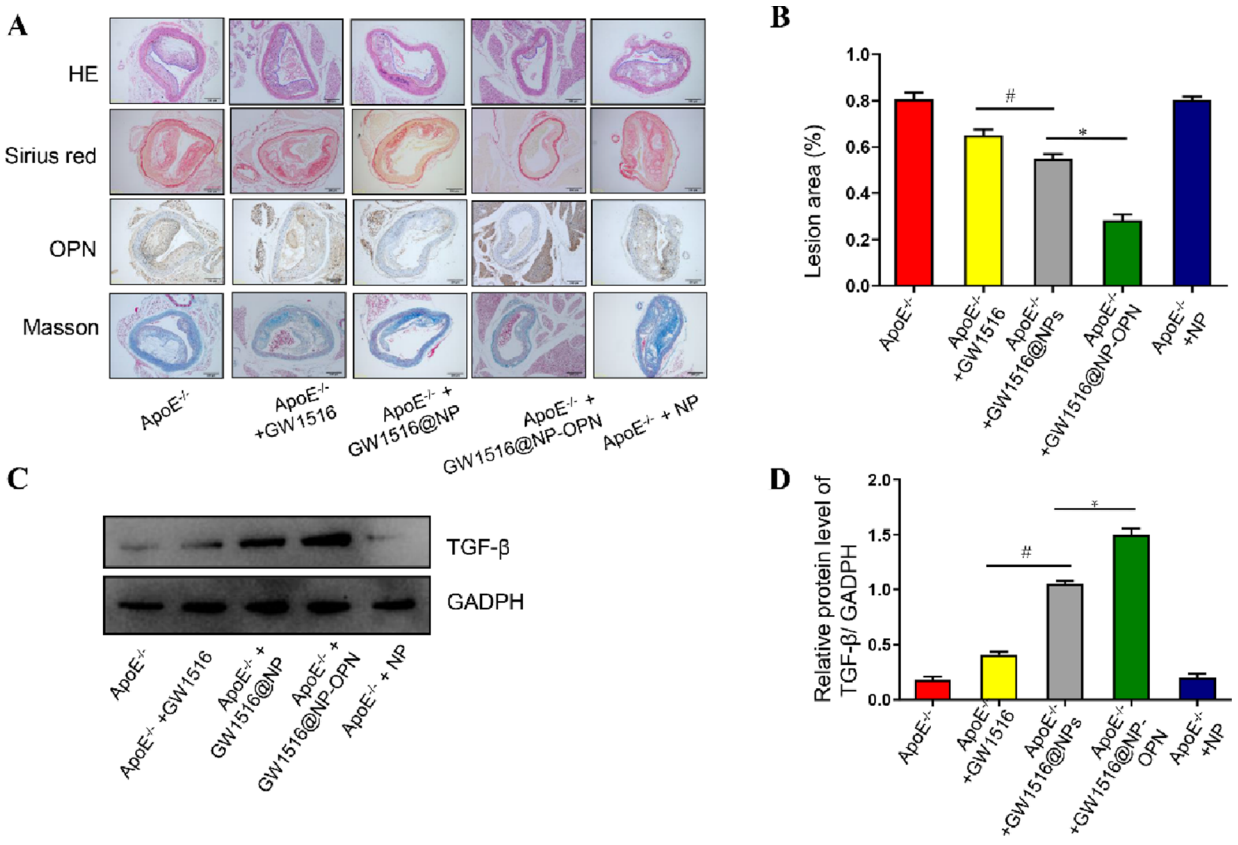

Figure 8. GW1516@NP-OPN inhibited the progression of atherosclerosis in ApoE$^{-/-}$ mice models in vivo. (A) H&E, Sirius red, OPN, and Masson staining demonstrate the atherosclerotic lesions directly. GW1516@NP-OPN-treated mice displayed the most favorable plaque phenotypes, in which the lesions had significantly smaller plaque sizes ($P < 0.05$) with smaller OPN contents ($P < 0.05$). (C) GW1516@NP-OPN markedly increased the expression of TGF-β in the plaque area vs free GW1516 ($P < 0.05$). (B) is the quantitative analysis of A and (D) is the quantitative analysis of C. Data are presented as mean ± SD ($n = 5$); scale bars = 200 μm.

physicochemical properties, including a smaller size, increased stability, and effective long circulation, compared to simple small molecules. It could prolong drug retention time in the aorta. The hydrodynamic size of GW1516@NP-OPN is about 40 nm larger than that of GW1516@NP. The incorporation of the antibody of OPN slightly increased their PDI. The targeted NP ζ potential is within the range of 0 to −18 MV (Figure 1D,E). The results are in agreement with previous findings.[46] It has been shown that micellar PEG has no charge or is negatively charged after connecting to antibodies.[47,48] The DLS results revealed that the drug loading and the linked antibody did not induce any aggregated precipitates. We found that the formula is not only stable for two weeks at 4 °C but also can be stored as a lyophilized powder at −20 °C for several months. Moreover, the attachment of antibodies to GW1516@NP-OPN had a slight effect on the EP and LE %, which is supported by the results of previously published data (Figure 2A).[49] One possible explanation for the difference in size and drug loading after linking antibodies is that the antibody is on the surface of the PEG hydrophilic chain, which makes the structure looser, larger in size, and smaller in drug loading.[25] All PEGylated nanoparticles show similar release characteristics, that is, the drug is the initial fast release to sustained release from the nanoparticles. The testing of GW1516 release from NPs revealed that the drug release rate of the OPN-targeted NP was slower than that of the non-targeted NPs (Figure 2B). The drug release rate may depend on the nature of the interstices in the nanoparticle structure. The smaller the interspace, the smoother the surface of the NP, and the lower the volume of drug that can be released. Our experimental results may be mediated by a covalent binding of micelles to antibodies. The binding may change the hydrophilic end structure and increase the size of interspaces.[25]

According to previous studies, targeted modified nanomedicines have more efficient pharmaceutical benefits with reduced toxicities.[51] The secreted protein OPN is highly expressed in smooth muscle cells in the middle and late stages of atherosclerosis and promotes the phenotypic transition of smooth muscle cells, making OPN an ideal molecular target that can effectively identify secreted VSMCs in atherosclerotic lesions.[51] Our group previously synthesized multiple OPN-antibody-linked NPs for the targeted imaging of vulnerable atherosclerotic plaques.[45,46] In the next step, we performed in vitro and in vivo imaging experiments for verifying the targeted properties. As was revealed in the results of flow cytometry and immunofluorescence, GW1516@NP-OPN presented higher selectivity toward VSMCs stimulated by ox-LDL (Figure 3A,B). An ex vivo fluorescence imaging study present obvious accumulations in atherosclerotic lesions in the ApoE$^{-/-}$ mice which were injected with targeted nanomaterials (Figure 7). Unfortunately, there is no immunofluorescence experiment to further verify the colocalization of nanomaterials with OPN.

In the next step, we applied the GW1516@NP-OPN in VSMCs treated with ox-LDL and HFD ApoE$^{-/-}$ mice for therapeutic purposes. Previous studies have shown that the stimulation by ox-LDL has been proved to be implicated in

https://doi.org/10.1021/acsomega.2c00575
ACS Omega 2022, 7, 28767−28778

VSMC apoptosis and migration. Although, PPARδ activation reduces ox-LDL induced apoptosis in VSMCs by modulating the TGF-β/FAK pathway in addition to inhibiting the migration, which affects cellular ROS production [14]. As shown by the vitro results, free GW1516 treatment inhibited cell migration and apoptosis in ox-LDL-induced VSMCs and then, GW1516@NP-OPN further diminished cell migration and apoptosis in ox-LDL-induced VSMCs compared with free GW1516. The migration ability of cells was assessed using the transwell system and scratch assays (Figure 4). Moreover, the flow cytometry analysis and the AO/EB staining assay revealed that compared with the free GW1516, GW1516@NP-OPN further reduced the rate of apoptotic cells induced by ox-LDL (Figure 5). In addition, the expression of MMP-2 and MMP-9 was detected in the present study, and the results found that GW1516@NP-OPN remarkably decreased the protein concentrations of MMP-2 and MMP-9 (Figure 6). Both MMP-2 and MMP-9 are important members of the MMP family. In addition to affecting the extracellular matrix to increase plaque instability, they could also mediate inflammatory cells, which is associated with cell migration. Notably, we also found that ox-LDL treatment significantly decreased protein concentrations of P-FAK and TGF-β1 in VSMCs; however, free GW1516 treatment increased their expression in ox-LDL-induced VSMCs and then, GW1516@NP-OPN further promoted the expression of P-FAK and TGF-β1 in ox-LDL-induced VSMCs compared with free GW1516 (Figure 6). At the same time, we verified that the therapeutic effect of the GW1516@NP-OPN could decrease plaque sizes and enhance stability (decreased necrotic core areas and OPN contents) more effectively in the histological results (Figure 8). In this context, the GW1516@NP-OPN-mediated delivery of GW1516 can facilitate the targeted delivery and improve the therapeutic efficacy of GW1516. This may be attributed to the targeted and long circulation properties of nanomedicines. To this end, we performed additional pharmacokinetic in vivo experiments to demonstrate the long circulation characteristics of GW1516@NPs-OPN compared to free drug GW1516. The results reveal that compared to free GW1516, the delayed T_{max} demonstrates an obvious sustained release of GW1516 in GW1516@NP-OPN. The increase in T_{max} indicates that GW1516@NP-OPN is eliminated more slowly in mice and has the long circulation effect. It is due to the fact that the free drug relies on the carrier for transport, the drug is released for a certain time and the PEG on nanoparticles improves the time in the blood circulation. It shows from the side that GW1516@NP-OPN prolongs the effective treatment time of GW1516 in mice to a certain extent (Figure S1).

However, to confirm the observed effects, it is required to verify these protein expression levels using PPARδ signaling inhibitors in future studies with NP. Other limitations of our study include the low number of mice tested in vivo, the limited testing of NP toxicity, and of NP signaling mechanisms in vitro. Additionally, further testing of nanoprobe colocalization within atherosclerotic plaques using immunological section analysis and confocal microscopy is required. Further studies are warranted to address these issues. In addition to the above-mentioned deficiencies in this study, it also includes the macrophage content and VSMC content of plaques were not analyzed. However, there is no denying that compared to administration of free agents, nanomedicines offer significant advantages in terms of stability, drug delivery efficiency, pharmacokinetics, targeting, safety, and versatility. In previous research, countless smart nanomedicines capable of precise functions have been created, relying on disease-specific tissue microenvironments and external stimuli. For example, in atherosclerotic plaques with elevated reactive oxygen species, we can make nanomaterials that release drugs in an intelligent response. In addition, we could use ultrasound, light, and so forth to trigger nanomedicines externally in local atherosclerotic plaque. We found that more and more chemo-physical strategies to increase the functionality of nanomedicine.[52]

5. CONCLUSIONS

In summary, the novel GW1516@NP-OPN can be efficiently absorbed by VSMCs and effectively diminish the development of atherosclerosis in cellular models in vitro and in mouse atherosclerotic plaque formation models in vivo through the TGF-β/FAK signaling axis, to inhibit the migration and apoptosis of VSMCs and the MMP activity. Thus, application of NPs indicates a promising advantage of this approach for targeted drug delivery in atherosclerosis treatment.

■ ASSOCIATED CONTENT

Supporting Information

The Supporting Information is available free of charge at https://pubs.acs.org/doi/10.1021/acsomega.2c00575.

Experimental methods and comparison of in vivo blood concentration studies of GW1516@NPs-OPN with the free drug GW1516 (PDF)

■ AUTHOR INFORMATION

Corresponding Authors

Chengchun Tang − *Department of Cardiology, Zhongda Hospital, School of Medicine, Southeast University, Nanjing, Jiangsu 210009, P.R. China*; Email: tangchengchun@hotmail.com

Feng Cao − *Department of Geriatric Cardiology, National Clinical Research Center for Geriatric Diseases, 2nd Medical Center, Chinese PLA General Hospital, Beijing 100853, China*; orcid.org/0000-0002-1010-6429; Email: fengcao8828@163.com

Authors

Xu Huang − *Department of Geriatric Cardiology, National Clinical Research Center for Geriatric Diseases, 2nd Medical Center, Chinese PLA General Hospital, Beijing 100853, China; Department of Cardiology, Zhongda Hospital, School of Medicine, Southeast University, Nanjing, Jiangsu 210009, P.R. China*

Yang Zhang − *Department of Geriatric Cardiology, National Clinical Research Center for Geriatric Diseases, 2nd Medical Center, Chinese PLA General Hospital, Beijing 100853, China*

Weiwei Zhang − *Nankai University School of Medicine, Nankai University, Tianjin 300073, China*

Cheng Qin − *Department of Geriatric Cardiology, National Clinical Research Center for Geriatric Diseases, 2nd Medical Center, Chinese PLA General Hospital, Beijing 100853, China*

Yan Zhu − *Nankai University School of Medicine, Nankai University, Tianjin 300073, China*

Yan Fang − *Department of Geriatric Cardiology, National Clinical Research Center for Geriatric Diseases, 2nd Medical*

Center, Chinese PLA General Hospital, Beijing 100853, China

Yabin Wang − *Department of Geriatric Cardiology, National Clinical Research Center for Geriatric Diseases, 2nd Medical Center, Chinese PLA General Hospital, Beijing 100853, China;* orcid.org/0000-0002-7966-6117

Complete contact information is available at: https://pubs.acs.org/10.1021/acsomega.2c00575

Author Contributions

X.H., C.T. and F.C. conceived and designed the study. Financial support was provided by Y.W. and F.C. Y.Z. and Y.F. performed the study; W.Z., C.Q., and Y.Z. analyzed the data; and X.H. wrote the paper.

Notes

The authors declare no competing financial interest.

■ ACKNOWLEDGMENTS

This work was supported by the Beijing Municipal Natural Science Foundation (7202189), National Nature Science Foundation of China (81530058, 81970443, 81671731, 81570272, 81571841, and 91939303), National Key Research Program of China (2016YFB0303303), NSFC Projects of International Cooperation and Exchanges (81820108019), Beijing Tianjin and Hebei Special Foundation (19JCZDJC63900), the Capital Clinical Feature Research Project (Z171100001017158), Big Data Program of Chinese PLA General Hospital (2017MBD-008), and Translational Medicine Program of Chinese PLA General Hospital (2017TM-003).

■ REFERENCES

(1) Libby, P.; Buring, J. E.; Badimon, L.; Hansson, G. K.; Deanfield, J.; Bittencourt, M. S.; Tokgözoğlu, L.; Lewis, E. F. Atherosclerosis. *Nat Rev Dis Primers.* **2019**, *5*, 56.

(2) Tarkin, J. M.; Dweck, M. R.; Evans, N. R.; Takx, R. A.; Brown, A. J.; Tawakol, A.; Fayad, Z. A.; Rudd, J. H. Imaging Atherosclerosis. *Circ. Res.* **2016**, *118*, 750−769.

(3) Aanei, I. L.; Huynh, T.; Seo, Y.; Francis, M. B. Vascular Cell Adhesion Molecule-Targeted MS2 Viral Capsids for the Detection of Early-Stage Atherosclerotic Plaques. *Bioconjug Chem* **2018**, *29*, 2526−2530.

(4) Muscari, A.; Puddu, G. M.; Puddu, P. Lipid-lowering drugs: are adverse effects predictable and reversible. *Cardiology* **2002**, *97*, 115−121.

(5) Wolak, T. Osteopontin - a multi-modal marker and mediator in atherosclerotic vascular disease. *Atherosclerosis* **2014**, *236*, 327−337.

(6) Liu, J.; Ren, Y.; Kang, L.; Zhang, L. Oxidized low-density lipoprotein increases the proliferation and migration of human coronary artery smooth muscle cells through the upregulation of osteopontin. *Int J Mol Med* **2014**, *33*, 1341−1347.

(7) Willis, A. I.; Pierre-Paul, D.; Sumpio, B. E.; Gahtan, V. Vascular smooth muscle cell migration: current research and clinical implications. *Vasc Endovascular Surg* **2004**, *38*, 11−23.

(8) Bennett, M. R.; Evan, G. I.; Schwartz, S. M. Apoptosis of human vascular smooth muscle cells derived from normal vessels and coronary atherosclerotic plaques. *J. Clin. Invest.* **1995**, *95*, 2266−2274.

(9) Libby, P.; Ridker, P. M.; Hansson, G. K. Progress and challenges in translating the biology of atherosclerosis. *Nature* **2011**, *473*, 317−325.

(10) Li, J.; Wang, H.; Shi, X.; Zhao, L.; Lv, T.; Yuan, Q.; Hao, W.; Zhu, J. Anti-proliferative and anti-migratory effects of Scutellaria strigillosa Hemsley extracts against vascular smooth muscle cells. *J Ethnopharmacol* **2019**, *235*, 155−163.

(11) Cormode, D. P.; Skajaa, T.; Fayad, Z. A.; Mulder, W. J. Nanotechnology in medical imaging: probe design and applications. *Arterioscler Thromb Vasc Biol* **2009**, *29*, 992−1000.

(12) Ross, R. Atherosclerosis–an inflammatory disease. *N. Engl. J. Med.* **1999**, *340*, 115−126.

(13) Mulder, W. J.; Jaffer, F. A.; Fayad, Z. A.; Nahrendorf, M. Imaging and nanomedicine in inflammatory atherosclerosis. *Sci Transl Med* **2014**, *6*, 239sr1.

(14) Hwang, J. S.; Eun, S. Y.; Ham, S. A.; Yoo, T.; Lee, W. J.; Paek, K. S.; Do, J. T.; Lim, D. S.; Seo, H. G. PPARδ modulates oxLDL-induced apoptosis of vascular smooth muscle cells through a TGF-β/FAK signaling axis. *Int. J. Biochem. Cell Biol.* **2015**, *62*, 54−61.

(15) Maltarollo, V. G.; Kronenberger, T.; Windshugel, B.; Wrenger, C.; Trossini, G.; Honorio, K. M. Advances and Challenges in Drug Design of PPARδ Ligands. *Curr. Drug Targets* **2018**, *19*, 144−154.

(16) Cheang, W. S.; Tian, X. Y.; Wong, W. T.; Huang, Y. The peroxisome proliferator-activated receptors in cardiovascular diseases: experimental benefits and clinical challenges. *Br. J. Pharmacol.* **2015**, *172*, 5512−5522.

(17) Lameijer, M. A.; Tang, J.; Nahrendorf, M.; Beelen, R. H.; Mulder, W. J. Monocytes and macrophages as nanomedicinal targets for improved diagnosis and treatment of disease. *Expert Rev Mol Diagn* **2013**, *13*, 567−580.

(18) Silva-Abreu, M.; Calpena, A. C.; Andrés-Benito, P.; Aso, E.; Romero, I. A.; Roig-Carles, D.; Gromnicova, R.; Espina, M.; Ferrer, I.; García, M. L.; Male, D. PPARγ agonist-loaded PLGA-PEG nanocarriers as a potential treatment for Alzheimer's disease: in vitro and in vivo studies. *Int J Nanomedicine* **2018**, *13*, 5577−5590.

(19) Ma, Q.; Yang, J.; Huang, X.; Guo, W.; Li, S.; Zhou, H.; Li, J.; Cao, F.; Chen, Y. Poly(Lactide-Co-Glycolide)-Monomethoxy-Poly-(Polyethylene Glycol) Nanoparticles Loaded with Melatonin Protect Adipose-Derived Stem Cells Transplanted in Infarcted Heart Tissue. *Stem Cells* **2018**, *36*, 540−550.

(20) Jiang, C.; Wang, H.; Zhang, X.; Sun, Z.; Wang, F.; Cheng, J.; Xie, H.; Yu, B.; Zhou, L. Deoxycholic acid-modified chitooligosaccharide/mPEG-PDLLA mixed micelles loaded with paclitaxel for enhanced antitumor efficacy. *Int. J. Pharm.* **2014**, *475*, 60−8.

(21) Liang, S.; Zheng, J.; Wu, W.; Li, Q.; Saw, P. E.; Chen, J.; Xu, X.; Yao, H.; Yao, Y. A Robust Nanoparticle Platform for RNA Interference in Macrophages to Suppress Tumor Cell Migration. *Front Pharmacol* **2018**, *9*, 1465.

(22) Wang, Y.; Zhang, Y.; Wang, Z.; Zhang, J.; Qiao, R. R.; Xu, M.; Yang, N.; Gao, L.; Qiao, H.; Gao, M.; Cao, F. Optical/MRI dual-modality imaging of M1 macrophage polarization in atherosclerotic plaque with MARCO-targeted upconversion luminescence probe. *Biomaterials* **2019**, *219*, 119378.

(23) Huang, X.; Xu, M. Q.; Zhang, W.; Ma, S.; Guo, W.; Wang, Y.; Zhang, Y.; Gou, T.; Chen, Y.; Liang, X. J.; Cao, F. ICAM-1-Targeted Liposomes Loaded with Liver X Receptor Agonists Suppress PDGF-Induced Proliferation of Vascular Smooth Muscle Cells. *Nanoscale Res. Lett.* **2017**, *12*, 322.

(24) Daneshmand, S.; Golmohammadzadeh, S.; Jaafari, M. R.; Movaffagh, J.; Rezaee, M.; Sahebkar, A.; Malaekeh-Nikouei, B. Encapsulation challenges, the substantial issue in solid lipid nanoparticles characterization. *J. Cell. Biochem.* **2018**, *119*, 4251−4264.

(25) Wang, F.; Chen, L.; Zhang, R.; Chen, Z.; Zhu, L. RGD peptide conjugated liposomal drug delivery system for enhance therapeutic efficacy in treating bone metastasis from prostate cancer. *J Control Release* **2014**, *196*, 222−233.

(26) Matsuo, K.; Suzuki, H.; Yatagai, N.; Enomoto, Y.; Kitayama, M.; Shigeoka, M.; Kimoto, A.; Matsumoto, K.; Komori, T. Red LED Light Is Influenced by IL-6 to Promote the Migration Ability of Oral Squamous Cell Carcinoma Cell Line. *Kobe J Med Sci* **2019**, *64*, E210−E216.

(27) Niu, J.; Li, X. M.; Wang, X.; Liang, C.; Zhang, Y. D.; Li, H. Y.; Liu, F. Y.; Sun, H.; Xie, S. Q.; Fang, D. DKK1 inhibits breast cancer cell migration and invasion through suppression of β-catenin/MMP7 signaling pathway. *Cancer Cell Int* **2019**, *19*, 168.

(28) Wang, W.; Zhu, M.; Xu, Z.; Li, W.; Dong, X.; Chen, Y.; Lin, B.; Li, M. Ropivacaine promotes apoptosis of hepatocellular carcinoma cells through damaging mitochondria and activating caspase-3 activity. *Biol Res* **2019**, *52*, 36.
(29) Ye, L.; Xiang, T.; Zhu, J.; Li, D.; Shao, Q.; Peng, W.; Tang, J.; Li, L.; Ren, G. Interferon Consensus Sequence-Binding Protein 8, a Tumor Suppressor, Suppresses Tumor Growth and Invasion of Non-Small Cell Lung Cancer by Interacting with the Wnt/β-Catenin Pathway. *Cell. Physiol. Biochem.* **2018**, *51*, 961−978.
(30) Wang, S. M.; Lin, H. Y.; Chen, Y. L.; Hsu, T. I.; Chuang, J. Y.; Kao, T. J.; Ko, C. Y. CCAAT/enhancer-binding protein delta regulates the stemness of glioma stem-like cells through activating PDGFA expression upon inflammatory stimulation. *J Neuroinflammation* **2019**, *16*, 146.
(31) Wu, Z.; Chen, C.; Zhang, B.; Tang, L.; Shi, W.; Liao, D.; Di, G.; Davis, J. R.; Wang, H. EGFP-EGF1-conjugated poly(lactic-co-glycolic acid) nanoparticles, a new diagnostic tool and drug carrier for atherosclerosis. *Int J Nanomedicine* **2019**, *14*, 2609−2618.
(32) Luo, C. J.; Luo, F.; Zhang, L.; Xu, Y.; Cai, G. Y.; Fu, B.; Feng, Z.; Sun, X. F.; Chen, X. M. Knockout of interleukin-17A protects against sepsis-associated acute kidney injury. *Ann Intensive Care* **2016**, *6*, 56.
(33) Wang, Y.; Chen, J.; Yang, B.; Qiao, H.; Gao, L.; Su, T.; Ma, S.; Zhang, X.; Li, X.; Liu, G.; Cao, J.; Chen, X.; Chen, Y.; Cao, F. In vivo MR and Fluorescence Dual-modality Imaging of Atherosclerosis Characteristics in Mice Using Profilin-1 Targeted Magnetic Nanoparticles. *Theranostics* **2016**, *6*, 272−286.
(34) Zhang, X. Q.; Even-Or, O.; Xu, X.; van Rosmalen, M.; Lim, L.; Gadde, S.; Farokhzad, O. C.; Fisher, E. A. Nanoparticles containing a liver X receptor agonist inhibit inflammation and atherosclerosis. *Adv Healthc Mater* **2015**, *4*, 228−236.
(35) Li, Z.; Qiao, W.; Wang, C.; Wang, H.; Ma, M.; Han, X.; Tang, J. DPPC-coated lipid nanoparticles as an inhalable carrier for accumulation of resveratrol in the pulmonary vasculature, a new strategy for pulmonary arterial hypertension treatment. *Drug Deliv* **2020**, *27*, 736−744.
(36) Yang, Y.; Yang, Y.; Xie, X.; Cai, X.; Zhang, H.; Gong, W.; Wang, Z.; Mei, X. PEGylated liposomes with NGR ligand and heat-activable cell-penetrating peptide-doxorubicin conjugate for tumor-specific therapy. *Biomaterials* **2014**, *35*, 4368−4381.
(37) Lyu, L.; Huang, L. Q.; Huang, T.; Xiang, W.; Yuan, J. D.; Zhang, C. H. Cell-penetrating peptide conjugates of gambogic acid enhance the antitumor effect on human bladder cancer EJ cells through ROS-mediated apoptosis. *Drug Des Devel Ther* **2018**, *12*, 743−756.
(38) Sommerville, L. J.; Kelemen, S. E.; Ellison, S. P.; England, R. N.; Autieri, M. V. Increased atherosclerosis and vascular smooth muscle cell activation in AIF-1 transgenic mice fed a high-fat diet. *Atherosclerosis* **2012**, *220*, 45−52.
(39) Xue, X. H.; Zhou, X. M.; Wei, W.; Chen, T.; Su, Q. P.; Tao, J.; Chen, L. D. Alisol A 24-Acetate, a Triterpenoid Derived from Alisma orientale, Inhibits Ox-LDL-Induced Phenotypic Transformation and Migration of Rat Vascular Smooth Muscle Cells through Suppressing ERK1/2 Signaling. *J Vasc Res* **2016**, *53*, 291−300.
(40) Frisch, S. M.; Vuori, K.; Ruoslahti, E.; Chan-Hui, P. Y. Control of adhesion-dependent cell survival by focal adhesion kinase. *J. Cell Biol.* **1996**, *134*, 793−799.
(41) Etheridge, M. L.; Campbell, S. A.; Erdman, A. G.; Haynes, C. L.; Wolf, S. M.; McCullough, J. The big picture on nanomedicine: the state of investigational and approved nanomedicine products. *Nanomedicine* **2013**, *9*, 1−14.
(42) Scharlach, C.; Kratz, H.; Wiekhorst, F.; Warmuth, C.; Schnorr, J.; Genter, G.; Ebert, M.; Mueller, S.; Schellenberger, E. Synthesis of acid-stabilized iron oxide nanoparticles and comparison for targeting atherosclerotic plaques: evaluation by MRI, quantitative MPS, and TEM alternative to ambiguous Prussian blue iron staining. *Nanomedicine* **2015**, *11*, 1085−1095.
(43) Tang, X.; Liang, Y.; Liu, X.; Zhou, S.; Liu, L.; Zhang, F.; Xie, C.; Cai, S.; Wei, J.; Zhu, Y.; Hou, W. PLGA-PEG Nanoparticles Coated with Anti-CD45RO and Loaded with HDAC Plus Protease Inhibitors Activate Latent HIV and Inhibit Viral Spread. *Nanoscale Res. Lett.* **2015**, *10*, 413.
(44) Franco, T. T.; Andrews, A. T.; Asenjo, J. A. Use of chemically modified proteins to study the effect of a single protein property on partitioning in aqueous two-phase systems: Effect of surface charge. *Biotechnol. Bioeng.* **1996**, *49*, 309−315.
(45) Kandulski, A.; Jechorek, D.; Caro, C.; Weigt, J.; Wex, T.; Mönkemüller, K.; Malfertheiner, P. Histomorphological differentiation of non-erosive reflux disease and functional heartburn in patients with PPI-refractory heartburn. *Aliment Pharmacol Ther* **2013**, *38*, 643−651.
(46) Bennett, M. R.; Sinha, S.; Owens, G. K. Vascular Smooth Muscle Cells in Atherosclerosis. *Circ. Res.* **2016**, *118*, 692−702.
(47) Ervinna, N.; Mita, T.; Yasunari, E.; Azuma, K.; Tanaka, R.; Fujimura, S.; Sukmawati, D.; Nomiyama, T.; Kanazawa, A.; Kawamori, R.; Fujitani, Y.; Watada, H. Anagliptin, a DPP-4 inhibitor, suppresses proliferation of vascular smooth muscles and monocyte inflammatory reaction and attenuates atherosclerosis in male apo E-deficient mice. *Endocrinology* **2013**, *154*, 1260−1270.
(48) Wang, B.; Ge, Z.; Cheng, Z.; Zhao, Z. Tanshinone IIA suppresses the progression of atherosclerosis by inhibiting the apoptosis of vascular smooth muscle cells and the proliferation and migration of macrophages induced by ox-LDL. *Biol Open* **2017**, *6*, 489−495.
(49) Sahebkar, A.; Chew, G. T.; Watts, G. F. New peroxisome proliferator-activated receptor agonists: potential treatments for atherogenic dyslipidemia and non-alcoholic fatty liver disease. *Expert Opin Pharmacother* **2014**, *15*, 493−503.
(50) Sharma, A. K.; Sk, S. k.; He, P.; Peters, J. M.; Amin, S. Synthesis of isosteric selenium analog of the PPARbeta/delta agonist GW1516 and comparison of biological activity. *Bioorg. Med. Chem. Lett.* **2010**, *20*, 4050−4052.
(51) Ganguly, R.; Wen, A. M.; Myer, A. B.; Czech, T.; Sahu, S.; Steinmetz, N. F.; Raman, P. Anti-atherogenic effect of trivalent chromium-loaded CPMV nanoparticles in human aortic smooth muscle cells under hyperglycemic conditions in vitro. *Nanoscale* **2016**, *8*, 6542−6554.
(52) Li, J.; Kataoka, K. Chemo-physical Strategies to Advance the in Vivo Functionality of Targeted Nanomedicine: The Next Generation. *J. Am. Chem. Soc.* **2021**, *143*, 538−559.

https://doi.org/10.1021/acsomega.2c00575
ACS Omega 2022, 7, 28767−28778